Proceedings of IMECE2007
2007 ASME International Mechanical Engineering Congress and Exposition
November 11-15, 2007, Seattle, Washington, USA

IMECE2007-42332

OBSERVER DESIGN FOR A STEAM REFORMER BASED SOLID OXIDE FUEL CELL SYSTEM WITH ANODE RECIRCULATION

Tuhin Das *
Visiting Assistant Professor
Dept. of Mechanical Engineering
Michigan State University
East Lansing, Michigan 48824
Email: tuhindas@egr.msu.edu

Ranjan Mukherjee
Professor
Dept. of Mechanical Engineering
Michigan State University
East Lansing, Michigan 48824
Email: mukherji@egr.msu.edu

ABSTRACT

In this paper we design an observer for online estimation of species concentrations in a steam reformer based Solid Oxide Fuel Cell (SOFC) system with anode recirculation and with methane as fuel. Since in SOFCs steam reforming occurs both in the reformer and in the fuel cell, a large number of concentration sensors are necessary for accurate control of critical performance variables such as utilization and steam-to-carbon-ratio. The purpose of the observer is to reduce the number of sensors required for control. In contrast to existing observers which are either designed for chemical reactors or for fuel cells exclusively, our design considers the coupled dynamics of the reformer and the fuel cell. We design an adaptive observer where the rates of reforming reactions are treated as slowly varying unknown parameters. Using a few concentration sensors we show that all other species concentrations, molar flow rates, and reaction rates in the fuel path can be dynamically estimated. Simulation results are provided in support of the proposed design.

NOMENCLATURE

C_p	Specific heat at constant pressure (J/kg/K)
C_s	Specific heat of solid volume (J/kg/K)
C_v	Specific heat at constant volume (J/kg/K)
E_a, E_b, E_c	Activation energy of reactions (a), (b), (c) in Eqns.(6) and (17) (J/mol)
F	Faraday's constant (= 96485.34 coulomb/mol)
h	Molar enthalpy (J/mole)
i	Current draw (amps)
k	Anode recirculation fraction
M_s	Mass of solid volume (kg)
N	Number of moles (moles)
N_c	Number of cells in series
$\dot{N}_{air}$	Molar flow rate of air (moles/sec)
$\dot{N}_f$	Molar flow rate of fuel (moles/sec)
$\dot{N}_{in}$	Anode inlet flow rate (moles/sec)
$\dot{N}_o$	Anode exit flow rate (moles/sec)
n	Number of electrons participating in electro-chemical reaction (= 2)
P_g	Control volume pressure (N/m^2)
p	Partial pressure (N/m^2)
$\dot{Q}_g$	Rate of heat transfer to gas control volume (W)
$\dot{Q}_s$	Rate of heat transfer to solid volume (W)
R_u	Universal Gas Constant (8.314J/mol/K)
r_a, r_b, r_c	Rates of reactions (a), (b), (c) in Eqns.(6) and (17) (mol/kg cat./sec)
r_d	Rate of electro-chemical reaction (moles/sec)
$STCR$	Steam-To-Carbon Ratio
T_g	Temperature of gas control volume (K)
T_{ref}	Reference temperature (K)
T_s	Temperature of solid volume (K)
V	Volume (m^3)
$\dot{W}_{net}$	Net work done (W)

*Address all correspondence to this author.

Symbols

ΔH	Enthalpy of reaction or adsorption (J/mol)
Δh_f^o	Enthalpy of formation at 298K and 1atm (J/mol)
$\mathcal{K}_a$, $\mathcal{K}_c$	Equilibrium constant of reactions (a) and (c) in Eqns.(6) and (17) (Pa^2)
$\mathcal{K}_b$	Equilibrium constant of reactions (b) in Eqns.(6) and (17)
$\mathcal{K}_{CH_4}$, $\mathcal{K}_{CO}$, $\mathcal{K}_{H_2}$	Adsorption constant for CH_4, CO, H_2 (Pa^{-1})
$\mathcal{K}_{H_2O}$	Adsorption constant for H_2O
κ_a, κ_c	Rate coefficient of reaction (a) and (c) (mol $Pa^{0.5}$/kg cat/sec)
κ_b	Rate coefficient of reaction (b) (mol/kg cat/sec/Pa)
$\dot{\eta}$	Molar flow rate (moles/sec)
$\mathcal{R}$	Species rate of formation (moles/sec)
$\mathcal{X}$	Species mole fraction

Subscripts

a	Anode control volume
c	Cathode control volume
cv	Generic control volume
e	Exit condition of control volume
in	Inlet condition of control volume
i	Values of 1 through 7 represent CH_4, CO, CO_2, H_2, H_2O, N_2, and O_2
r	Reformate control volume

INTRODUCTION

Among different fuel cell technologies, Solid Oxide Fuel Cells (SOFC) have attracted research interests due to several factors. SOFC systems are solid state devices that are simpler in concept than other fuel cell technologies. Fuel flexibility and tolerance to impurities are attractive features of SOFCs. High temperature operating conditions (800 to 1000°C) of SOFCs are conducive to internal reforming of fuels and the exhaust gases are excellent means for sustaining on-board fuel reforming. SOFCs are not only tolerant to carbon monoxide but can also use it as fuel and this simplifies the fuel reforming systems. Furthermore, high operating temperatures makes SOFC-Gas Turbine hybrids excellent combined heat and power (CHP) systems.

For optimal performance of SOFC systems, well designed control strategies must be implemented. A critical variable in SOFCs is fuel utilization. High utilization implies high efficiency, however, too high a utilization results in reduced partial pressure of hydrogen that leads to diminished cell voltage and can cause irreversible damages to the fuel cell due to anode oxidation, (1). Steam-To-Carbon-Ratio (STCR) is a critical performance variable in steam-reformer based SOFC systems. STCR indicates the availability of sufficient steam for fuel reforming at the reformer inlet. An STCR greater than the stoichiometric ratio of steam and carbon is necessary since an inlet flow lean in steam causes catalyst deactivation through carbon deposition, (2). Hence control of utilization and STCR are necessary for the overall efficiency and longevity of the system.

Since utilization and STCR are functions of species concentrations, sensors to measure the same are necessary in implementing control algorithms. The reforming process in SOFCs essentially generates a hydrogen rich gas by breaking down complex hydrocarbon molecules into simpler ones. Furthermore, the reforming process occurs in two stages, first in the reformer, and second in the fuel cell itself. Steam reforming of methane leads to five major components in the fuel path, namely, CH_4, CO, CO_2, H_2 and H_2O, with different concentrations in the reformer and in the fuel cell. Hence, online computation of utilization and STCR would require a large number of concentration sensors which would significantly increase costs and complicate the hardware. A means of reducing concentration sensors is to use observers that dynamically estimate species concentrations from online sensor data using a mathematical model.

We design an observer for a steam reformer based tubular SOFC system with anode recirculation and methane as fuel. We develop a lumped control-oriented model that captures the details of heat and mass transfer, chemical kinetics and electro-chemical phenomena of the system. Our control-oriented model has similarities with the tubular SOFC models developed in (3) and (1). The kinetics of steam reforming are modeled based on the experimental results in (4). Other tubular SOFC system models appear in (5), (6), (7) and (8) and models of planar SOFC systems appear in (9) and references therein.

Literature review reveals that although there are several publications in observer designs for chemical reactors, (10), there are few that address observer design in fuel cells, (11). These designs focus on either chemical reactors or fuel cells exclusively. A unique aspect of our observer design is that we consider the coupled dynamics of the steam reformer and the fuel cell. This is necessary since, for our SOFC system, a fraction of the anode exit flow is recirculated into the reformer to supply steam for the steam reforming process. The observers in (10), (12) and (13) rely on temperature dynamics for estimation. In our observer design, although temperature measurements are utilized, we refrain from using the temperature dynamics of the SOFC system. This is because high temperature operating conditions can result in significant heat exchange through radiative means or otherwise due to the specific layout of hardware, which would remain unmodeled. Similarly, although pressure measurements are utilized, we neglect the pressure dynamics of the system, (1). Several designs such as (12), (13), and (14) assume prior knowledge of reaction rates. However, in (15) and (16), the authors show estimation errors arising from uncertain reaction rate parameters and adopt an adaptive approach for estimating these parameters. In (10), the observer design is based on coordinate transformations that eliminate reaction rate terms. In our

adaptive observer design, we treat the rates of steam reforming reactions as slowly varying unknown parameters. This assumption is based on slow temperature dynamics of SOFC systems, preferred uniform temperature operation of SOFCs to prevent thermal stresses, and strong temperature dependence of reaction rates, and is confirmed through simulations. In (11), the authors have designed an adaptive observer for hydrogen estimation in a Polymer Electrolyte Membrane (PEM) fuel cell. The observer considers the inlet hydrogen partial pressure as a slowly varying unknown parameter and uses voltage measurements. For the PEM system, the only reaction in the fuel cell is the electrochemical conversion of hydrogen to water. In contrast, for the SOFC system, in addition to the electrochemical conversion of hydrogen to steam, direct internal reforming of methane is also accounted for. A total of eight reaction rate and molar flow rate parameters are identified of which four independent parameters are extracted and estimated by the observer.

This paper is organized as follows. In our discussion on the SOFC model development, we first describe the SOFC system. In the subsequent section we develop the mathematical model of the SOFC system in three main subsections. We first present the equations for the fundamental gas and solid control volume models. The next subsections describe the steam reformer and SOFC system models. We focus primarily on the mass transfer phenomena and chemical kinetics. Although not elaborated in our discussion, the heat transfer phenomena of the system is modeled in detail but omitted here for the sake of brevity. An open-loop simulation of the system model is provided next. Subsequently, the development of adaptive observer designs for reformer based SOFC systems is demonstrated through a sample observer design. A stability analysis is presented next. Simulation results are provided in the following section. Finally, conluding remarks are provided followed by references.

SOFC MODEL DEVELOPMENT

SOFC System Description

In this section, we describe the steam reformer based tubular SOFC system which forms the basis of our analysis. The SOFC system is outlined in Fig.1. Methane is chosen as the fuel for the system, with a molar flow rate of $\dot{N}_f$. The reformer produces a hydrogen-rich gas which is supplied to the anode of the SOFC stack. Electrochemical reactions occuring at the anode due to current draw results in a steam-rich gas-mixture at the anode exit. A fraction k of the anode efflux is recirculated into the reformer through a mixing chamber where fuel is added. The mixing of the two fluid streams and pressurization is achieved using an ejector or a recirculating fuel pump, (2), (17). The steam reforming process occuring in the reformer catalyst bed is an endothermic process. The energy required to sustain the process is supplied from two sources, namely, the combustor efflux that is passed through the reformer, and the aforementioned recirculated flow which is also passed through the reformer before being injected into the mixing chamber, as shown in Fig.1. The remaining anode efflux is mixed with the cathode outflow in the combustion chamber. The combustor also serves to preheat the cathode air flow which has a molar flow rate of $\dot{N}_{air}$. The tubular construction of each cell causes the air to first enter the cell through the air supply tube and then reverse its direction to enter the cathode chamber. The cathode air serves as the source of oxygen for the fuel cell.

SOFC System Model

Fundamental Models The essential dynamics of the SOFC system in Fig.1 can be captured through the fundamental solid volume and gas control volume models.

Solid Volume Model: The thermodynamics of a solid volume can be expressed as

$$M_s C_s \dot{T}_s = \dot{Q}_s \tag{1}$$

Conductive and convective heat transfers are modeled using Fourier's Law and Newton's law respectively, (1).

Gas Control Volume: The gas control volume model consists of energy and mass balance equations. Additonally, it captures the reaction kinetics arising from fuel reforming and electrochemistry. Throughout the model, gas composition and flow rate information are transmitted among control volumes using a uniform signal bus. Signals one through seven of the bus denote the seven relevant components, namely CH_4, CO, CO_2, H_2, H_2O, N_2, and O_2 respectively. The energy balance equation implemented for the generic gaseous control volume containing a gas mixture is

$$N_{cv} C_v \dot{T}_g = \dot{\eta}_{in} h_{in} - \dot{\eta}_e h_e + \dot{Q}_g - \dot{W}_{net} \tag{2}$$

The species mass balance equation is constructed as follows,

$$N_{cv} \dot{\mathcal{X}}_{i,cv} = \dot{\eta}_{in} \mathcal{X}_{i,in} - \dot{\eta}_e \mathcal{X}_{i,cv} + \mathcal{R}_{i,cv}, \quad i = 1,2,\cdots,7 \tag{3}$$

where the subscripts i, $i = 1,2,\cdots,7$, correspond to the species CH_4, CO, CO_2, H_2, H_2O, N_2, and O_2 respectively. From Eqn.(3), we additionally have

$$\sum_{i=1}^{7} \mathcal{X}_{i,in} = \sum_{i=1}^{7} \mathcal{X}_{i,cv} = 1 \Rightarrow \sum_{i=1}^{7} \dot{\mathcal{X}}_{i,cv} = 0 \Rightarrow \dot{\eta}_e = \dot{\eta}_{in} + \sum_{i=1}^{7} \mathcal{R}_{i,cv} \tag{4}$$

In our formulation the states of the gaseous control volume model are T_g and $\mathcal{X}_{i,cv}$, $i = 1,2,\cdots,7$. Flow is assumed to be

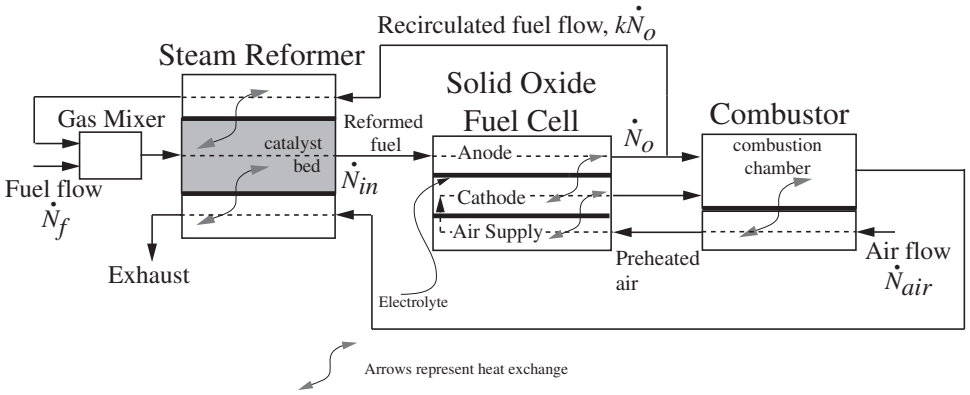

Figure 1. SCHEMATIC OF THE SOFC SYSTEM

governed by a nominal pressure drop across each module, (1), and hence is not treated as a state variable. The gas mixture is assumed to satisfy ideal gas laws and hence N_{cv} in Eqns.(2) and (3) is related to P_g and T_g through $N_{cv} = P_g V_{cv}/R_u T_g$. In Eqn.(2), C_v, h_{in}, and h_e are related to the state variables through:

$$\begin{aligned} C_v(T) &= \sum_{i=1}^{7} \mathcal{X}_i C_{p,i}(T) - R_u, \\ \tfrac{C_{p,i}(T)}{R_u} &= a_i + b_i T + c_i T^2 + d_i T^3 + e_i T^4, \\ h &= \sum_{i=1}^{7} \mathcal{X}_i \left(\int_{298}^{T} C_{p,i}(T)\, dT + \Delta h^o_{f,i} \right) \end{aligned} \tag{5}$$

$C_{p,i}$ is expressed in functional form using the coefficients a_i, b_i, c_i, d_i, e_i, as given in (18). The inlet and exit enthalpies are computed using inlet temperature T_{in} and exit temperature $T_e = T_g$.

Reformer Model For steam reforming of methane we consider a packed-bed tubular reformer with nickel-alumina catalyst, (19). A schematic diagram of the steam reformer is shown in Fig.2. The exhaust, steam and reformate flows are modeled using gas control volumes and the catalyst bed is modeled as a solid volume. The details of heat transfer characteristics of the system is given in (1) and is not repeated here. Instead, we emphasize on the reformer reaction kinetics and mass transfer phenomena.

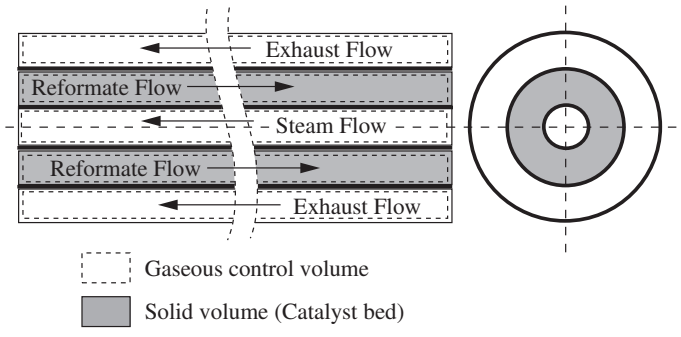

Figure 2. SCHEMATIC OF TUBULAR STEAM REFORMER

The three main reactions that simultaneously occur during steam reforming of methane, (3), (4), are:

$$\begin{aligned} &(a) \quad CH_4 + H_2O \leftrightarrow CO + 3H_2 \\ &(b) \quad CO + H_2O \leftrightarrow CO_2 + H_2 \\ &(c) \quad CH_4 + 2H_2O \leftrightarrow CO_2 + 4H_2 \end{aligned} \tag{6}$$

We use the following reaction rate expressions, given in (4), to model the reformer kinetics:

$$r_a = \frac{\kappa_a}{p_{H_2}^{2.5}} \left(p_{CH_4} p_{H_2O} - \frac{p_{H_2}^3 p_{CO}}{\mathcal{K}_a} \right) \Big/ \delta^2 \tag{7}$$

$$r_b = \frac{\kappa_b}{p_{H_2}} \left(p_{CO} p_{H_2O} - \frac{p_{H_2} p_{CO_2}}{\mathcal{K}_b} \right) \Big/ \delta^2 \tag{8}$$

$$r_c = \frac{\kappa_c}{p_{H_2}^{3.5}} \left(p_{CH_4} p_{H_2O}^2 - \frac{p_{H_2}^4 p_{CO_2}}{\mathcal{K}_c} \right) \Big/ \delta^2 \tag{9}$$

where

$$\begin{aligned} &\delta = 1 + \mathcal{K}_{CO} p_{CO} + \mathcal{K}_{H_2} p_{H_2} + \mathcal{K}_{CH_4} p_{CH_4} + \mathcal{K}_{H_2O} p_{H_2O} p_{H_2}, \\ &p_{\bar{q}} = \mathcal{X}_{\bar{q}} P,\ \bar{q} = CH_4, CO, CO_2, H_2, H_2O \end{aligned} \tag{10}$$

In Eqns.(7), (8) and (9), κ_a, κ_b, and κ_c are given by

$$\kappa_j = \kappa_{j,T_{ref}} \exp\left[-\frac{E_j}{R_u} \left(\frac{1}{T} - \frac{1}{T_{ref}} \right) \right], \quad j = a, b, c, \tag{11}$$

and $\mathcal{K}_{CO}$, $\mathcal{K}_{H_2}$, $\mathcal{K}_{CH_4}$, $\mathcal{K}_{H_2O}$ are expressed as

$$\mathcal{K}_q = \mathcal{K}_{q,T_{ref}} \exp\left[-\frac{\Delta H_q}{R_u}\left(\frac{1}{T}-\frac{1}{T_{ref}}\right)\right], q = CO, H_2, CH_4, H_2O \tag{12}$$

The values of T_{ref}, $\kappa_{j,T_{ref}}$, $\mathcal{K}_{q,T_{ref}}$, E_j and ΔH_q are given in (4). From the reforming reaction (a), (b) and (c) in Eqn.(6), we have

$$\begin{array}{ll} \mathcal{R}_{1,r} = -(r_a + r_c), & \mathcal{R}_{2,r} = (r_a - r_b), \\ \mathcal{R}_{3,r} = (r_b + r_c), & \mathcal{R}_{4,r} = (3r_a + r_b + 4r_c), \\ \mathcal{R}_{5,r} = -(r_a + r_b + 2r_c), & \mathcal{R}_{6,r} = 0, \\ \mathcal{R}_{7,r} = 0 & \end{array} \tag{13}$$

where r_a, r_b and r_c are computed using reformer temperature T_r, pressure P_r, mole fractions $\mathcal{X}_{\bar{q},r}$ and the total catalyst mass in the packed bed reformer. In Eqn.(13), any two of $\mathcal{R}_{1,r}$, $\mathcal{R}_{2,r}$, $\mathcal{R}_{3,r}$, $\mathcal{R}_{4,r}$ and $\mathcal{R}_{5,r}$ are independent. In general, for the reforming reactions in Eqn.(6), it can be shown that the rates of formation of any two of CH_4, CO, CO_2, H_2 and H_2O determine the rate of formation of the rest. Considering the rate of formation of CH_4 and CO in the reformer to be independent variables, we can write

$$\mathcal{R}_{3,r} = -\mathcal{R}_{1,r} - \mathcal{R}_{2,r},\ \mathcal{R}_{4,r} = -4\mathcal{R}_{1,r} - \mathcal{R}_{2,r},\ \mathcal{R}_{5,r} = 2\mathcal{R}_{1,r} + \mathcal{R}_{2,r} \tag{14}$$

Referring to Fig.1 and from Eqns.(3) and (14), the mass balance equations for CH_4, CO, CO_2, H_2 and H_2O can be written as

$$\begin{array}{l} N_r \dot{\mathcal{X}}_{1,r} = k\dot{N}_o \mathcal{X}_{1,a} - \dot{N}_{in}\mathcal{X}_{1,r} + \mathcal{R}_{1,r} + \dot{N}_f \\ N_r \dot{\mathcal{X}}_{2,r} = k\dot{N}_o \mathcal{X}_{2,a} - \dot{N}_{in}\mathcal{X}_{2,r} + \mathcal{R}_{2,r} \\ N_r \dot{\mathcal{X}}_{3,r} = k\dot{N}_o \mathcal{X}_{3,a} - \dot{N}_{in}\mathcal{X}_{3,r} - \mathcal{R}_{1,r} - \mathcal{R}_{2,r} \\ N_r \dot{\mathcal{X}}_{4,r} = k\dot{N}_o \mathcal{X}_{4,a} - \dot{N}_{in}\mathcal{X}_{4,r} - 4\mathcal{R}_{1,r} - \mathcal{R}_{2,r} \\ N_r \dot{\mathcal{X}}_{5,r} = k\dot{N}_o \mathcal{X}_{5,a} - \dot{N}_{in}\mathcal{X}_{5,r} + 2\mathcal{R}_{1,r} + \mathcal{R}_{2,r} \end{array} \tag{15}$$

with $N_r = P_r V_r / R_u T_r$. Note that the reformer inlet and exit flows, as shown in Fig.1, do not contain O_2 and N_2. As a result, $\mathcal{X}_{6,r} = \mathcal{X}_{7,r} = 0$. From Eqns.(4) and (15) we deduce that

$$\dot{N}_{in} = k\dot{N}_o + \dot{N}_f + \sum_{i=1}^{7} \mathcal{R}_{i,r} \quad \Rightarrow \quad \dot{N}_{in} = k\dot{N}_o + \dot{N}_f - 2\mathcal{R}_{1,r} \tag{16}$$

SOFC Model Tubular Solid Oxide Fuel Cells are considered for our system analysis. A schematic diagram of an SOFC is shown in Fig.3. The anode, cathode and feed air flows are modeled using gas control volumes. The air feed tube and the electrolyte are modeled as solid volumes. Details of the heat transfer characteristics of these control volumes and voltage computations are given in (1) and is not repeated here. Instead, we emphasize on the fuel cell chemical kinetics and mass transfer phenomena as in the previous section.

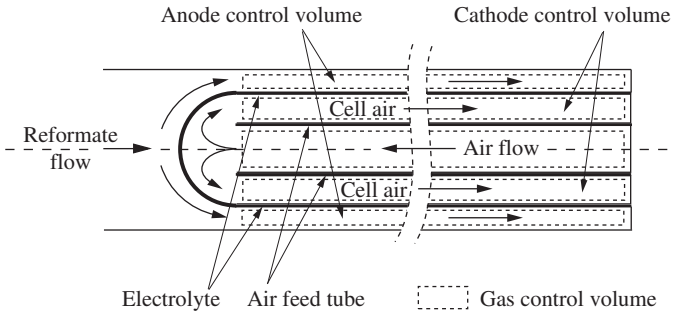

Figure 3. SCHEMATIC DIAGRAM OF TUBULAR SOFC

Anode control volume: The following chemical and electrochemical reactions are considered in the anode volume:

$$\begin{array}{ll} (a) & CH_4 + H_2O \leftrightarrow CO + 3H_2 \\ (b) & CO + H_2O \leftrightarrow CO_2 + H_2 \\ (c) & CH_4 + 2H_2O \leftrightarrow CO_2 + 4H_2 \\ (d) & H_2 + O^{2-} \rightarrow H_2O + 2e \end{array} \tag{17}$$

The occurance of the reactions (a), (b) and (c) are due to internal reforming in the anode control volume which is aided by the elevated cell temperatures in SOFC and due to the presence of nickel catalyst in the anode. Electrochemical conversion of CO to CO_2 at the anode is also possible in parallel to the electrochemical process of steam generation from H_2. However, as pointed out in (20) and references therein, this reaction is much slower in presence of reactions (b) and (d) in Eqn.(17) and is therefore ignored in our analysis.

The rate of internal reforming reactions in the anode control volume, namely (a), (b) and (c), are modeled as given in Eqn.(9). The rate coefficients κ_j and the adsorption constants $\mathcal{K}_q$ in Eqns.(11) and (12) are calculated with T_a instead of T_g. The rate of electrochemical reaction (d) is given as

$$r_d = \frac{iN_c}{nF} \tag{18}$$

The rates of formation of the individual gas species in the anode control volume are expressed as follows

$$\begin{array}{ll} \mathcal{R}_{1,a} = -(r_a + r_c), & \mathcal{R}_{2,a} = (r_a - r_b), \\ \mathcal{R}_{3,a} = (r_b + r_c), & \mathcal{R}_{4,a} = (3r_a + r_b + 4r_c) - r_d, \\ \mathcal{R}_{5,a} = -(r_a + r_b + 2r_c) + r_d, & \mathcal{R}_{6,a} = 0, \\ \mathcal{R}_{7,a} = 0 & \end{array} \tag{19}$$

For the anode, r_a, r_b and r_c are computed using Eqns.(7), (8), (9), (10), (11), (12), with temperature T_a, pressure P_a, mole fractions $\mathcal{X}_{\bar{q},a}$ and using the anode catalyst mass. As shown in Eqn.(14),

with $\mathcal{R}_{1,a}$, $\mathcal{R}_{2,a}$ and r_d as independent variables, we have

$$\begin{aligned}\mathcal{R}_{3,a} &= -\mathcal{R}_{1,r} - \mathcal{R}_{2,r},\\ \mathcal{R}_{4,a} &= -4\mathcal{R}_{1,r} - \mathcal{R}_{2,r} - r_d,\\ \mathcal{R}_{5,a} &= 2\mathcal{R}_{1,r} + \mathcal{R}_{2,r} + r_d\end{aligned} \tag{20}$$

Referring to Fig.1 and from Eqns.(3) and (20), the mass balance equations for CH_4, CO, CO_2, H_2 and H_2O can be written as:

$$\begin{aligned}N_a\dot{\mathcal{X}}_{1,a} &= -\dot{N}_o\mathcal{X}_{1,a} + \dot{N}_{in}\mathcal{X}_{1,r} + \mathcal{R}_{1,a}\\ N_a\dot{\mathcal{X}}_{2,a} &= -\dot{N}_o\mathcal{X}_{2,a} + \dot{N}_{in}\mathcal{X}_{2,r} + \mathcal{R}_{2,a}\\ N_a\dot{\mathcal{X}}_{3,a} &= -\dot{N}_o\mathcal{X}_{3,a} + \dot{N}_{in}\mathcal{X}_{3,r} - \mathcal{R}_{1,a} - \mathcal{R}_{2,a}\\ N_a\dot{\mathcal{X}}_{4,a} &= -\dot{N}_o\mathcal{X}_{4,a} + \dot{N}_{in}\mathcal{X}_{4,r} - 4\mathcal{R}_{1,a} - \mathcal{R}_{2,a} - r_d\\ N_a\dot{\mathcal{X}}_{5,a} &= -\dot{N}_o\mathcal{X}_{5,a} + \dot{N}_{in}\mathcal{X}_{5,r} + 2\mathcal{R}_{1,a} + \mathcal{R}_{2,a} + r_d\end{aligned} \tag{21}$$

with $N_a = P_aV_a/R_uT_a$. As with the reformate control volume, the anode inlet and exit flows, do not contain O_2 and N_2. Therefore, $\mathcal{X}_{6,r} = \mathcal{X}_{7,r} = 0$, and hence we disregard the mass balance equations of N_2 and O_2. From Eqns.(4) and (21) we deduce that

$$\dot{N}_o = \dot{N}_{in} + \sum_{i=1}^{7}\mathcal{R}_{i,a} \quad \Rightarrow \quad \dot{N}_o = \dot{N}_{in} - 2\mathcal{R}_{1,a} \tag{22}$$

Cathode control volume: The electro-chemical conversion of O_2 to O^{2-} ions takes place in the cathode control volume.

$$\frac{1}{2}O_2 + 2e \rightarrow O^{2-} \tag{23}$$

with the reaction rate as given in Eqn.(18). Considering the mole fractions of N_2 and O_2 in air to be 0.79 and 0.21 respectively, the mass balance equations of the cathode control volume can be written from Eqns.(18) and (23) as follows:

$$\begin{aligned}N_c\dot{\mathcal{X}}_{6,c} &= 0.79\dot{N}_{air} - \left(\dot{N}_{air} - \tfrac{r_d}{2}\right)\mathcal{X}_{6,c}\\ N_c\dot{\mathcal{X}}_{7,c} &= 0.21\dot{N}_{air} - \left(\dot{N}_{air} - \tfrac{r_d}{2}\right)\mathcal{X}_{7,c} - \tfrac{r_d}{2}\\ \mathcal{X}_{i,c} &= 0, \quad i = 1,2,\cdots,5\end{aligned} \tag{24}$$

Simulations

In this section we provide results of open-loop simulation of the SOFC system model. We consider a system with 100 cells in series, a fuel (pure CH_4) flow of 0.0034 moles/sec, air flow of 0.035 moles/sec, and a recirculation of 69%. The simulation results are shown in Fig.4. The load current is changed in steps as shown in Fig.4(a). The cell voltage and temperature changes corresponding to the changes in the current are shown Figs.4(b) and (d). Figs.4(e) and (f) depict the mole fractions of the species at reformer exit and anode exit respectively. The H_2O concentration is higher and the H_2 concentration is lower at the anode exit in comparison to the reformer exit. This is an expected outcome of the electro-chemical reactions resulting from current draw. The near equilibrium condition of the Water-Gas-Shift reaction in the anode (reaction (c) of Eqn.(17)) is evident through the sharp depletion of CO corresponding to the depletion of H_2 due to the current draw, as shown in Fig.4(f), especially around 500s to 700s when the current demand was maximum. Internal reforming in the anode control volume is illustrated by the negligible concentration of CH_4 at the anode exit in Fig.4(f).

In Fig.4(c), utilization and steam-to-carbon ratio (STCR) are depicted. Utilization is defined as the difference in the H_2 availability between the inlet and exit flows of the anode over the net H_2 availability at the anode inlet. STCR is defined as the ratio of concentration of steam molecules to that of carbon atoms in the inlet of the reformer.

OBSERVER DESIGN

Problem Statement

The observer design problem statement is as follows: Given that temperatures and pressures can be sensed in the reformer and anode volumes, and given that the fuel cell current can be measured, design a procedure for online estimation of rates of steam reformation reactions, molar flow rates and species concentrations using a minimum number of concentration sensors.

Observer Equations

In this section we state the equations for a sample observer design where CH_4 and CO concentrations are sensed in the reformer and anode volumes, i.e., measurements of $\mathcal{X}_{1,r}$, $\mathcal{X}_{1,a}$, $\mathcal{X}_{2,r}$, $\mathcal{X}_{2,a}$ are assumed to be available. Note that this choice is arbitrary and similar observers can be designed by sensing any two of CH_4, CO, CO_2, H_2, and H_2O in the reformer and anode volumes. Our nonlinear observer design is based on Lyapunov function approach and the observer equations are designed to guarantee uniform asymptotic stability of the observer error dynamics. From Eqns.(15), (16), (21) and (22), the variables to be estimated are chosen as $\dot{N}_{in}$, $\dot{N}_o$, $\mathcal{R}_{2,r}$, $\mathcal{R}_{2,a}$, $\mathcal{X}_{i,r}$, $\mathcal{X}_{i,a}$, $i = 1,2,\cdots,5$. Their estimates are denoted by $\hat{\dot{N}}_{in}$, $\hat{\dot{N}}_o$, $\hat{\mathcal{R}}_{2,r}$, $\hat{\mathcal{R}}_{2,a}$, $\hat{\mathcal{X}}_{i,r}$, $\hat{\mathcal{X}}_{i,a}$, $i = 1,2,\cdots,5$. Solving Eqns.(16) and (22) for $\mathcal{R}_{1,r}$ and $\mathcal{R}_{1,a}$, substituting into Eqns.(15) and (21), and replacing $\mathcal{X}_{1,r}$, $\mathcal{X}_{1,a}$, $\mathcal{X}_{2,r}$, $\mathcal{X}_{2,a}$, $\dot{N}_{in}$, $\dot{N}_o$, $\mathcal{R}_{2,r}$ and $\mathcal{R}_{2,a}$ with their estimates, we have the following observer equations:

$$\begin{aligned}N_r\dot{\hat{\mathcal{X}}}_{1,r} &= k\hat{\dot{N}}_o\left(\hat{\mathcal{X}}_{1,a} + 0.5\right) - \hat{\dot{N}}_{in}\left(\hat{\mathcal{X}}_{1,r} + 0.5\right) + \mathcal{L}_{1,r}\,\mathcal{E}_{1,r} + 1.5\dot{N}_f\\ N_a\dot{\hat{\mathcal{X}}}_{1,a} &= -\hat{\dot{N}}_o\left(\hat{\mathcal{X}}_{1,a} + 0.5\right) + \hat{\dot{N}}_{in}\left(\hat{\mathcal{X}}_{1,r} + 0.5\right) + \mathcal{L}_{1,a}\,\mathcal{E}_{1,a}\\ N_r\dot{\hat{\mathcal{X}}}_{2,r} &= k\hat{\dot{N}}_o\hat{\mathcal{X}}_{2,a} - \hat{\dot{N}}_{in}\hat{\mathcal{X}}_{2,r} + \hat{\mathcal{R}}_{2,r} + \mathcal{L}_{2,r}\,\mathcal{E}_{2,r}\\ N_a\dot{\hat{\mathcal{X}}}_{2,a} &= -\hat{\dot{N}}_o\hat{\mathcal{X}}_{2,a} + \hat{\dot{N}}_{in}\hat{\mathcal{X}}_{2,r} + \hat{\mathcal{R}}_{2,a} + \mathcal{L}_{2,a}\,\mathcal{E}_{2,a}\end{aligned} \tag{25}$$

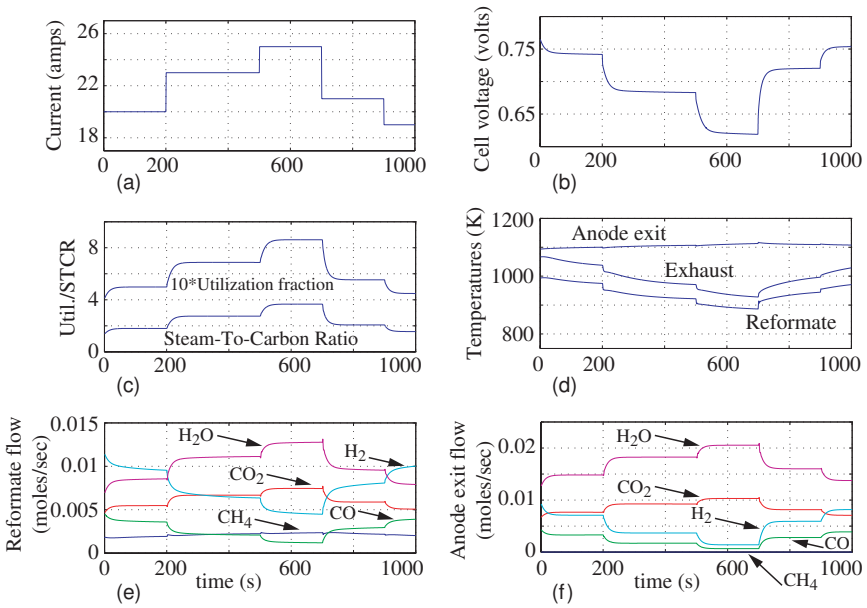

Figure 4. OPEN-LOOP SIMULATION OF STEAM REFORMER BASED SOFC SYSTEM

Note that the extra terms $\mathcal{L}_{1,r}\mathcal{E}_{1,r}$, $\mathcal{L}_{1,a}\mathcal{E}_{1,a}$, $\mathcal{L}_{2,r}\mathcal{E}_{2,r}$ and $\mathcal{L}_{2,a}\mathcal{E}_{2,a}$ are added to guarantee stability of the error dynamics as shown in the next section. As discussed in the introduction, we treat $\dot{N}_{in}$, $\dot{N}_o$, $\mathcal{R}_{2,r}$ and $\mathcal{R}_{2,a}$ as slowly varying unknown parameters and design the following parameter adaptation laws

$$\begin{aligned}
\dot{\hat{N}}_{in} &= \gamma_1\left[(\mathcal{E}_{1,a}-\mathcal{E}_{1,r})\left(\hat{\mathcal{X}}_{1,r}+0.5\right)+(\mathcal{E}_{2,a}-\mathcal{E}_{2,r})\hat{\mathcal{X}}_{2,r}\right]\\
\dot{\hat{N}}_{o} &= \gamma_2\left[(k\mathcal{E}_{1,r}-\mathcal{E}_{1,a})\left(\hat{\mathcal{X}}_{1,a}+0.5\right)+(k\mathcal{E}_{2,r}-\mathcal{E}_{2,a})\hat{\mathcal{X}}_{2,a}\right]\\
\dot{\hat{\mathcal{R}}}_{2,r} &= \gamma_3\mathcal{E}_{2,r}\\
\dot{\hat{\mathcal{R}}}_{2,a} &= \gamma_4\mathcal{E}_{2,a}
\end{aligned} \tag{26}$$

where, $\gamma_1,\gamma_2,\gamma_3,\gamma_4>0$, $\mathcal{L}_{1,r},\mathcal{L}_{1,a},\mathcal{L}_{2,r},\mathcal{L}_{2,a}>0$, and

$$\begin{aligned}
\mathcal{E}_{1,r}=\mathcal{X}_{1,r}-\hat{\mathcal{X}}_{1,r},\quad \mathcal{E}_{1,a}=\mathcal{X}_{1,a}-\hat{\mathcal{X}}_{1,a},\\
\mathcal{E}_{2,r}=\mathcal{X}_{2,r}-\hat{\mathcal{X}}_{2,r},\quad \mathcal{E}_{2,a}=\mathcal{X}_{2,a}-\hat{\mathcal{X}}_{2,a},\\
\mathcal{L}_{1,r}=\mathcal{L}_{1,a}=\mathcal{L}_{2,r}=\mathcal{L}_{2,a}=0.5\sup\left(\left|\dot{N}_o-\dot{N}_{in}\right|\right)
\end{aligned} \tag{27}$$

Using the parameter estimates in Eqn.(26), the remaining species concentrations are estimated using the following observer equations derived from Eqns.(15), (16), (18), (21) and (22):

$$\begin{aligned}
N_r\dot{\hat{\mathcal{X}}}_{3,r} &= k\hat{\dot{N}}_o\left(\hat{\mathcal{X}}_{3,a}-0.5\right)-\hat{\dot{N}}_{in}\left(\hat{\mathcal{X}}_{3,r}-0.5\right)-0.5\dot{N}_f-\hat{\mathcal{R}}_{2,r}\\
N_r\dot{\hat{\mathcal{X}}}_{4,r} &= k\hat{\dot{N}}_o\left(\hat{\mathcal{X}}_{4,a}-2\right)-\hat{\dot{N}}_{in}\left(\hat{\mathcal{X}}_{4,r}-2\right)-2\dot{N}_f-\hat{\mathcal{R}}_{2,r}\\
N_r\dot{\hat{\mathcal{X}}}_{5,r} &= k\hat{\dot{N}}_o\left(\hat{\mathcal{X}}_{5,a}+1\right)-\hat{\dot{N}}_{in}\left(\hat{\mathcal{X}}_{5,r}-1\right)+\dot{N}_f+\hat{\mathcal{R}}_{2,r}\\
N_a\dot{\hat{\mathcal{X}}}_{3,a} &= -\hat{\dot{N}}_o\left(\hat{\mathcal{X}}_{3,a}-0.5\right)+\hat{\dot{N}}_{in}\left(\hat{\mathcal{X}}_{3,r}-0.5\right)-\hat{\mathcal{R}}_{2,a}\\
N_a\dot{\hat{\mathcal{X}}}_{4,a} &= -\hat{\dot{N}}_o\left(\hat{\mathcal{X}}_{4,a}-2\right)+\hat{\dot{N}}_{in}\left(\hat{\mathcal{X}}_{4,r}-2\right)-\hat{\mathcal{R}}_{2,a}-\tfrac{iN_c}{nF}\\
N_a\dot{\hat{\mathcal{X}}}_{5,a} &= -\hat{\dot{N}}_o\left(\hat{\mathcal{X}}_{5,a}+1\right)+\hat{\dot{N}}_{in}\left(\hat{\mathcal{X}}_{5,r}+1\right)+\hat{\mathcal{R}}_{2,a}+\tfrac{iN_c}{nF}
\end{aligned} \tag{28}$$

Stability Analysis

We now prove the stability of the parameter and state estimation errors for this observer through application of the concept of input-to-state stability, (21) for cascaded systems. We consider the following groups of parameter and state estimation errors:

$$\begin{aligned}
\mathbf{E}_1 &= \left[\mathcal{E}_{1,r}\ \mathcal{E}_{1,a}\ \mathcal{E}_{2,r}\ \mathcal{E}_{2,a}\ \mathcal{E}_{\dot{N}_{in}}\ \mathcal{E}_{\dot{N}_o}\ \mathcal{E}_{\mathcal{R}_{2,r}}\ \mathcal{E}_{\mathcal{R}_{2,a}}\right]^T\\
\mathbf{E}_2 &= \left[\mathcal{E}_{3,r}\ \mathcal{E}_{3,a}\right]^T,\ \mathbf{E}_3=\left[\mathcal{E}_{4,r}\ \mathcal{E}_{4,a}\right]^T,\ \mathbf{E}_4=\left[\mathcal{E}_{5,r}\ \mathcal{E}_{5,a}\right]^T
\end{aligned} \tag{29}$$

where $\mathcal{E}_{1,r}$, $\mathcal{E}_{1,a}$, $\mathcal{E}_{2,r}$, $\mathcal{E}_{2,a}$ are given in Eqn.(27) and

$$\begin{aligned}
\mathcal{E}_{\dot{N}_{in}}=\dot{N}_{in}-\hat{\dot{N}}_{in},\quad \mathcal{E}_{\dot{N}_o}=\dot{N}_o-\hat{\dot{N}}_o,\\
\mathcal{E}_{\mathcal{R}_{2,r}}=\mathcal{R}_{2,r}-\hat{\mathcal{R}}_{2,r},\ \mathcal{E}_{\mathcal{R}_{2,a}}=\mathcal{R}_{2,a}-\hat{\mathcal{R}}_{2,a}
\end{aligned}$$

$$\begin{aligned}
\mathcal{E}_{3,r}=\mathcal{X}_{3,r}-\hat{\mathcal{X}}_{3,r},\ \mathcal{E}_{4,r}=\mathcal{X}_{4,r}-\hat{\mathcal{X}}_{4,r},\ \mathcal{E}_{5,r}=\mathcal{X}_{5,r}-\hat{\mathcal{X}}_{5,r}\\
\mathcal{E}_{3,a}=\mathcal{X}_{3,a}-\hat{\mathcal{X}}_{3,a},\ \mathcal{E}_{4,a}=\mathcal{X}_{4,a}-\hat{\mathcal{X}}_{4,a},\ \mathcal{E}_{5,a}=\mathcal{X}_{5,a}-\hat{\mathcal{X}}_{5,a}
\end{aligned} \tag{30}$$

The error dynamics can be derived from Eqns.(15), (16), (21), (22), (25), (26), and (28), and are given below

$$\begin{aligned}
N_r\dot{\mathcal{E}}_{1,r} &= k\dot{N}_o\mathcal{E}_{1,a}-\dot{N}_{in}\mathcal{E}_{1,r}-\mathcal{L}_{1,r}\mathcal{E}_{1,r}-\mathcal{E}_{\dot{N}_{in}}\left(\hat{\mathcal{X}}_{1,r}+0.5\right)\\
&\quad +k\mathcal{E}_{\dot{N}_o}\left(\hat{\mathcal{X}}_{1,a}+0.5\right)\\
N_a\dot{\mathcal{E}}_{1,a} &= -\dot{N}_o\mathcal{E}_{1,a}+\dot{N}_{in}\mathcal{E}_{1,r}-\mathcal{L}_{1,a}\mathcal{E}_{1,a}+\mathcal{E}_{\dot{N}_{in}}\left(\hat{\mathcal{X}}_{1,r}+0.5\right)\\
&\quad -\mathcal{E}_{\dot{N}_o}\left(\hat{\mathcal{X}}_{1,a}+0.5\right)\\
N_r\dot{\mathcal{E}}_{2,r} &= k\dot{N}_o\mathcal{E}_{2,a}-\dot{N}_{in}\mathcal{E}_{2,r}-\mathcal{L}_{2,r}\mathcal{E}_{2,r}+\mathcal{E}_{\mathcal{R}_{2,r}}-\mathcal{E}_{\dot{N}_{in}}\hat{\mathcal{X}}_{2,r}\\
&\quad +k\mathcal{E}_{\dot{N}_o}\hat{\mathcal{X}}_{2,a}\\
N_a\dot{\mathcal{E}}_{2,a} &= -\dot{N}_o\mathcal{E}_{2,a}+\dot{N}_{in}\mathcal{E}_{2,r}-\mathcal{L}_{2,a}\mathcal{E}_{2,a}+\mathcal{E}_{\mathcal{R}_{2,a}}+\mathcal{E}_{\dot{N}_{in}}\hat{\mathcal{X}}_{2,r}\\
&\quad -\mathcal{E}_{\dot{N}_o}\hat{\mathcal{X}}_{2,a}
\end{aligned} \tag{31}$$

$$
\begin{aligned}
N_r\dot{\mathcal{E}}_{3,r} &= k\dot{N}_o\mathcal{E}_{3,a} - \dot{N}_{in}\mathcal{E}_{3,r} - \mathcal{E}_{\dot{N}_{in}}\left(\hat{\mathcal{X}}_{3,r} - 0.5\right) \\
&\quad + k\mathcal{E}_{\dot{N}_o}\left(\hat{\mathcal{X}}_{3,a} - 0.5\right) - \mathcal{E}_{\mathcal{R}_{2,r}} \\
N_a\dot{\mathcal{E}}_{3,a} &= -\dot{N}_o\mathcal{E}_{3,a} + \dot{N}_{in}\mathcal{E}_{3,r} + \mathcal{E}_{\dot{N}_{in}}\left(\hat{\mathcal{X}}_{3,r} - 0.5\right) \\
&\quad - \mathcal{E}_{\dot{N}_o}\left(\hat{\mathcal{X}}_{3,a} - 0.5\right) - \mathcal{E}_{\mathcal{R}_{2,a}} \\
N_r\dot{\mathcal{E}}_{4,r} &= k\dot{N}_o\mathcal{E}_{4,a} - \dot{N}_{in}\mathcal{E}_{4,r} - \mathcal{E}_{\dot{N}_{in}}\left(\hat{\mathcal{X}}_{4,r} - 2\right) \\
&\quad + k\mathcal{E}_{\dot{N}_o}\left(\hat{\mathcal{X}}_{4,a} - 2\right) - \mathcal{E}_{\mathcal{R}_{2,r}} \\
N_a\dot{\mathcal{E}}_{4,a} &= -\dot{N}_o\mathcal{E}_{4,a} + \dot{N}_{in}\mathcal{E}_{4,r} + \mathcal{E}_{\dot{N}_{in}}\left(\hat{\mathcal{X}}_{4,r} - 2\right) \\
&\quad - \mathcal{E}_{\dot{N}_o}\left(\hat{\mathcal{X}}_{4,a} - 2\right) - \mathcal{E}_{\mathcal{R}_{2,a}} \\
N_r\dot{\mathcal{E}}_{5,r} &= k\dot{N}_o\mathcal{E}_{5,a} - \dot{N}_{in}\mathcal{E}_{5,r} - \mathcal{E}_{\dot{N}_{in}}\left(\hat{\mathcal{X}}_{5,r} + 1\right) \\
&\quad + k\mathcal{E}_{\dot{N}_o}\left(\hat{\mathcal{X}}_{5,a} + 1\right) + \mathcal{E}_{\mathcal{R}_{2,r}} \\
N_a\dot{\mathcal{E}}_{5,a} &= -\dot{N}_o\mathcal{E}_{5,a} + \dot{N}_{in}\mathcal{E}_{5,r} + \mathcal{E}_{\dot{N}_{in}}\left(\hat{\mathcal{X}}_{5,r} + 1\right) \\
&\quad - \mathcal{E}_{\dot{N}_o}\left(\hat{\mathcal{X}}_{5,a} + 1\right) + \mathcal{E}_{\mathcal{R}_{2,a}}
\end{aligned}
\tag{32}
$$

The error dynamics of the parameter estimates can be obtained from Eqn.(26) using the substitution

$$
\dot{\mathcal{E}}_{\dot{N}_{in}} = -\dot{\hat{N}}_{in},\ \dot{\mathcal{E}}_{\dot{N}_o} = -\dot{\hat{N}}_o,\ \dot{\mathcal{E}}_{\mathcal{R}_{2,r}} = -\dot{\hat{\mathcal{R}}}_{2,r},\ \dot{\mathcal{E}}_{\mathcal{R}_{2,a}} = -\dot{\hat{\mathcal{R}}}_{2,a} \tag{33}
$$

The state variable descriptions of $\mathbf{E}_1$ through $\mathbf{E}_4$ can now be expressed in the cascaded form

$$
\dot{\mathbf{E}}_1 = f_1(\mathbf{E}_1), \tag{34}
$$

$$
\dot{\mathbf{E}}_2 = f_2(\mathbf{E}_1, \mathbf{E}_2), \tag{35}
$$

$$
\dot{\mathbf{E}}_3 = f_3(\mathbf{E}_1, \mathbf{E}_3), \tag{36}
$$

$$
\dot{\mathbf{E}}_4 = f_4(\mathbf{E}_1, \mathbf{E}_4) \tag{37}
$$

We prove global uniform asymptotic stability of the origin of the cascaded system in Eqns.(34), (35), (36) and (37) by applying Lemma 4.7 and Lemma 4.6 of (21). According to Lemma 4.7 of (21), the cascaded system given by Eqns.(34), (35), (36) and (37) satisfies the above stability property if,

1. The origin of Eqn.(34) is globally uniformly asymptotically stable, and
2. The origins of Eqns.(35), (36) and (37), with $\mathbf{E}_1$ as input, are input-to-state stable.

To prove the first condition, we choose the following Lyapunov function candidate:

$$
\begin{aligned}
V = \tfrac{1}{2}\Big[&N_r\mathcal{E}_{1,r}^2 + N_a\mathcal{E}_{1,a}^2 + N_r\mathcal{E}_{2,r}^2 + N_a\mathcal{E}_{2,a}^2 \\
&+ \tfrac{1}{\gamma_1}N_r\mathcal{E}_{\dot{N}_{in}}^2 + \tfrac{1}{\gamma_2}N_a\mathcal{E}_{\dot{N}_o}^2 + \tfrac{1}{\gamma_3}N_r\mathcal{E}_{\mathcal{R}_{2,r}}^2 + \tfrac{1}{\gamma_4}N_a\mathcal{E}_{\mathcal{R}_{2,a}}^2\Big]
\end{aligned}
\tag{38}
$$

Due to internal steam reforming in anode volume $\dot{N}_o \geq \dot{N}_{in}$ and therefore $\sup\left(\left|\dot{N}_o - \dot{N}_{in}\right|\right) > \left(\dot{N}_o - \dot{N}_{in}\right)$. From Eqns.(38), (26), (27), (31), and (33), defining $\mathcal{Z}_1 = \mathcal{E}_{1,r}/\mathcal{E}_{1,a}$ and $\mathcal{Z}_2 = \mathcal{E}_{2,r}/\mathcal{E}_{2,a}$, we can write

$$
\begin{aligned}
\dot{V} &= -\mathcal{E}_{1,a}^2\left[\left(\dot{N}_{in} + \mathcal{L}_{1,r}\right)\mathcal{Z}_1^2 + \left(\dot{N}_o + \mathcal{L}_{1,a}\right) - \left(k\dot{N}_o + \dot{N}_{in}\right)\mathcal{Z}_1\right] \\
&\quad - \mathcal{E}_{2,a}^2\left[\left(\dot{N}_{in} + \mathcal{L}_{2,r}\right)\mathcal{Z}_2^2 + \left(\dot{N}_o + \mathcal{L}_{2,a}\right) - \left(k\dot{N}_o + \dot{N}_{in}\right)\mathcal{Z}_2\right] \\
&< -\mathcal{E}_{1,a}^2\left[0.5\left(\dot{N}_{in} + \dot{N}_o\right)\mathcal{Z}_1^2 + 0.5\left(\dot{N}_{in} + \dot{N}_o\right) - \left(k\dot{N}_o + \dot{N}_{in}\right)\mathcal{Z}_1\right] \\
&\quad - \mathcal{E}_{2,a}^2\left[0.5\left(\dot{N}_{in} + \dot{N}_o\right)\mathcal{Z}_2^2 + 0.5\left(\dot{N}_{in} + \dot{N}_o\right) - \left(k\dot{N}_o + \dot{N}_{in}\right)\mathcal{Z}_2\right] \\
&\leq 0
\end{aligned}
\tag{39}
$$

Indeed, the Lyapunov function V in Eqn.(38) is a radially unbounded, continuously differentiable, positive definite, decrescent function whose derivative along the system trajectories is negative definite as shown in Eqn.(39). Furthermore, the properties above hold globally and this establishes the global uniform asymptotic stability of the origin of Eqn.(34). Note that the design of parameter adaptation laws in Eqn.(26) and the choice of the observer gains $\mathcal{L}_{1,r}$, $\mathcal{L}_{1,a}$, $\mathcal{L}_{2,r}$, $\mathcal{L}_{2,a}$ in Eqn.(27) directly contributes in ensuring $\dot{V} \leq 0$. To prove the second condition above, we apply Lemma 4.6 of (21). We now show that the origin of Eqn.(35), with $\mathbf{E}_1$ as input, is input-to-state stable. For the systems in Eqns.(36) and (37), the proofs are omitted for brevity. According to Lemma 4.6 of (21), we need to prove global exponential stability of $\mathbf{E}_2 = \mathbf{0}$ for the unforced system $\dot{\mathbf{E}}_2 = f_2(\mathbf{0}, \mathbf{E}_2)$. From Eqn.(32), the unforced system is given by

$$
\begin{bmatrix} \dot{\mathcal{E}}_{3,r} \\ \dot{\mathcal{E}}_{3,a} \end{bmatrix} = \begin{bmatrix} -\frac{\dot{N}_{in}}{N_r} & \frac{k\dot{N}_o}{N_r} \\ \frac{\dot{N}_{in}}{N_a} & -\frac{\dot{N}_o}{N_a} \end{bmatrix} \begin{bmatrix} \mathcal{E}_{3,r} \\ \mathcal{E}_{3,a} \end{bmatrix} \quad \Rightarrow \quad \dot{\mathbf{E}}_2 = \mathbf{A}_{\mathbf{E}_2}\mathbf{E}_2, \tag{40}
$$

treating the recirculation fraction k as a known constant parameter with $0 < k < 1$. It can be verified that $\mathbf{A}_{\mathbf{E}_2}$ is Hurwitz and, in fact, the eigenvalues of $\mathbf{A}_{\mathbf{E}_2}$ are real and negative and this establishes the global exponential stability of the unforced system. Hence, the origin of Eqn.(35), with $\mathbf{E}_1$ as input, is input-to-state stable. Thus, by satisfying both the conditions mentioned above, we have established global uniform asymptotic stability of the origin of the cascaded system given in Eqns.(34), (35), (36) and (37), and this implies stability of the error dynamics.

SIMULATIONS

We provide simulation results in support of the observer design in the sections above. We perform an open loop simulation of the system model with $\dot{N}_f = 0.0097$moles/s, $\dot{N}_a = 0.098$moles/s and a recirculation fraction $k = 0.75$. The current demand was changed in steps as given below

$$
i = \begin{cases} 50 \text{ for } \ 0 \leq t < 100 \\ 70 \text{ for } 100 \leq t < 200 \\ 40 \text{ for } 200 \leq t \leq 300 \end{cases} \tag{41}
$$

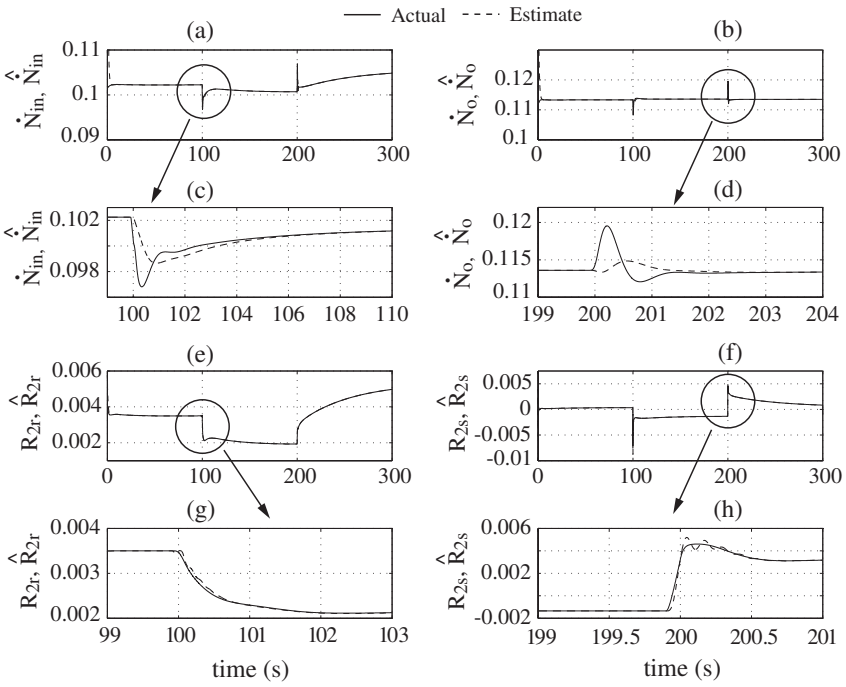

Figure 6. $\dot{N}_{in}$, $\dot{N}_o$, $\mathcal{R}_{2,r}$, $\mathcal{R}_{2,s}$ AND THEIR ESTIMATES

As per the design of the observer, we assume that molar fractions CH_4 and CO are sensed in the reformer and anode control volumes. The sensed and estimated molar fractions of CH_4 and CO in the reformer and anode control volumes are plotted in Fig.(5). The values of the observer gains are chosen as $\mathcal{L}_{1,r} = \mathcal{L}_{1,a} = \mathcal{L}_{2,r} = \mathcal{L}_{2,a} = 1$ and $\gamma_1 = \gamma_2 = \gamma_3 = \gamma_4 = 250$. The values of γ_1, γ_2, γ_3 and γ_4 determine the rate of convergence of $\dot{N}_{in}$, $\dot{N}_o$, $\mathcal{R}_{2,r}$ and $\mathcal{R}_{2,s}$. The estimates of $\dot{N}_{in}$, $\dot{N}_o$, $\mathcal{R}_{2,r}$ and $\mathcal{R}_{2,s}$, and their model-generated actual values are plotted in Fig.6. In Figs.6(c) and 6(d) the plots of $\dot{N}_{in}$ and $\dot{N}_o$ and their estimates are magnified around 100s and 200s respectively. Similarly, in Figs.6(g) and 6(h) the plots of $\mathcal{R}_{2,r}$ and $\mathcal{R}_{2,s}$ and their estimates are magnified around 100s and 200s respectively. The observer estimates of the unknown species concentrations of CO_2, H_2, and H_2O, in the reformer and the anode control volumes and their model-generated actual values are plotted in Fig.7.

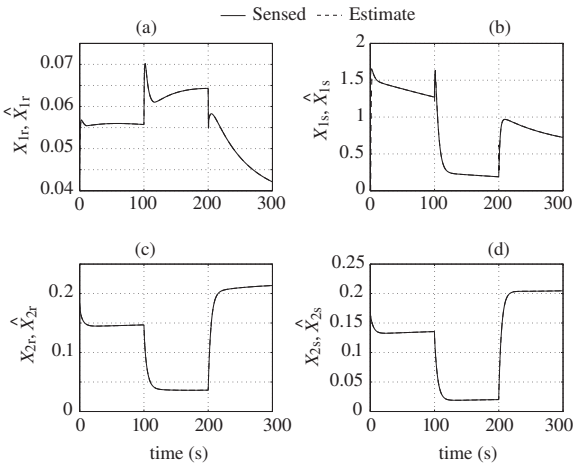

Figure 5. CH_4 AND CO MOLE FRACTIONS AT REFORMER AND ANODE EXITS

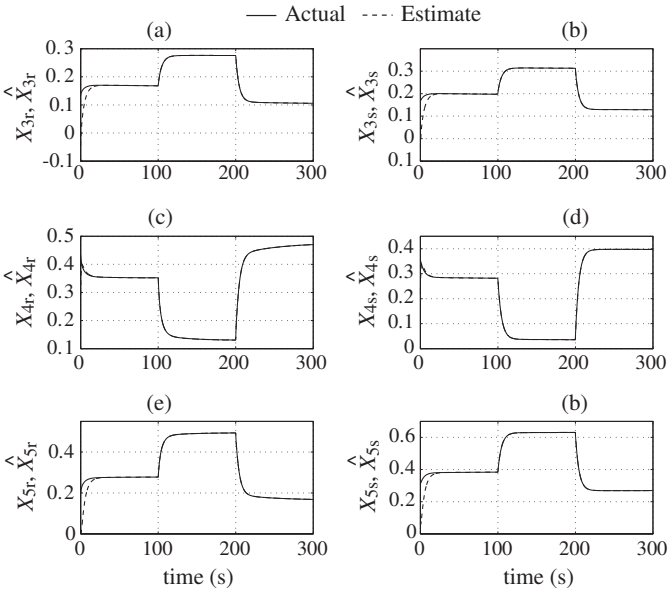

Figure 7. CO_2, H_2, H_2O MOLE FRACTIONS AND THEIR ESTIMATES

CONCLUSION

In this paper we have designed an adaptive observer for an SOFC system with anode recirculation and with methane as the fuel. In the proposed design we have shown that the net molar flow rates, reaction rates and all species concentrations in the reformer and the anode control volumes can be estimated by sensing the concentrations of any two species in the reformer and the same two species in the anode volumes. The specific design presented in this paper assumes CH_4 and CO sensors to be available, however any other combination is equally effective. Temperature and pressure measurements at the reformer and anode exits are assumed to be available, however their dynamics are not considered in the observer design. We prove stability of the observer using the notion of input-to-state stability of cascaded systems. In our stability analysis we treat the recirculation fraction as a constant. In our future work we shall attempt to relax this condition. Furthermore, we shall also attempt to use voltage measurements and thereby further reduce the number of concentrations sensors necessary for the observer. This paper develops a theoretical framework for observer design for reformer based SOFC systems. Experimental validation of this design approach will be pursued in future research.

REFERENCES

[1] Mueller, F., Brouwer, J., Jabbari, F., and Samuelsen, S., 2006. "Dynamic simulation of an integrated solid oxide fuel cell system including current-based fuel flow control". *ASME Journal of Fuel Cell Science and Technology*, **3**, pp. 144–154.

[2] Ferrari, M. L., Traverso, A., Magistri, L., and Massardo, A. F., 2005. "Influence of anodic recirculation transient behavior on the sofc hybrid system performance". *Journal of Power Sources*, **149**, pp. 22–32.

[3] Kandepu, R., Imsland, L., Foss, B. A., Stiller, C., Thorud, B., and Bolland, O., 2007. "Modeling and control of a sofc-gt-based autonomous power system". *Energy*, **32**, pp. 406–417.

[4] Xu, J., and Froment, G. F., 1989. "Methane steam reforming, methanation and water-gas shift: I. intrinsic kinetics". *AIChE Journal*, **35**(1), pp. 88–96.

[5] Hall, D. J., and Colclaser, R. G., 1999. "Transient modeling and simulation of a tubular solid oxide fuel cell". *IEEE Transactions on Energy Conversion*, **14**(3), pp. 749–753.

[6] Lazzaretto, A., Toffolo, A., and Zanon, F., 2004. "Parameter setting for a tubular sofc simulation model". *ASME Journal of Energy Resources Technology*, **126**, pp. 40–46.

[7] Li, P., and Chyu, M. K., 2003. "Simulation of the chemical/electrochemical reactions and heat/mass transfer for a tubular sofc in a stack". *Journal of Power Sources*, **124**, pp. 487–498.

[8] Xue, X., Tang, J., Sammes, N., and Du, Y., 2005. "Dynamic modeling of single tubular sofc combining heat/mass transfer and electrochemical reaction effects". *Journal of Power Sources*, **142**, pp. 211–222.

[9] Xi, H., Sun, J., and Tsourapas, V., 2007. "A control oriented low order dynamic model for planar sofc using minimum gibbs free energy method". *Journal of Power Sources*, **165**, pp. 253–266.

[10] Gorgun, H., Arcak, M., Varigonda, S., and Bortoff, S. A., 2005. "Observer designs for fuel processing reactors in fuel cell power systems". *International Journal of Hydrogen Energy*, **30**, pp. 447–457.

[11] Arcak, M., Gorgun, H., Pedersen, L. M., and Varigonda, S., 2004. "A nonlinear observer design for fuel cell hydrogen estimation". *IEEE TRansactions on Control Systems Technology*, **12**(1), pp. 101–110.

[12] Gibon-Fargeot, A. M., Hammouri, H., and Celle, F., 1994. "Nonlinear observers for chemical reactors". *Chemical Engineering Science*, **49**(14), pp. 2287–2300.

[13] Iyer, N. M., and Farell, A. E., 1996. "Design of a stable adaptive nonlinear observer for an exothermic stirred tank reactor". *Computers Chemical Engineering*, **20**(9), pp. 1141–1147.

[14] Soroush, M., 1997. "Nonlinear state-observer design with application to reactors". *Chemical Engineering Science*, **52**(3), pp. 387–404.

[15] Dochain, D., 2003. "State observers for processes with uncertain kinetics". *International Journal of Control*, **76**(15), pp. 1483–1492.

[16] Perrier, M., de Azevedo, S. F., Ferreira, E. C., and Dochain, D., 2000. "Tuning of observer-based estimators: Theory and application to the on-line estimation of kinetic parameters". *Control Engineering Practice*, **8**, pp. 377–388.

[17] Karnik, A. Y., and Sun, J., 2005. "Modeling and control of an ejector based anode recirculation system for fuel cells". *Proceedings of ASME Fuel Cell 2005*, pp. 721–731.

[18] Wark, K., 1988. *Thermodynamics*, fifth ed. McGraw-Hill, Inc., New York, NY.

[19] Incropera, F. P., and DeWitt, D. P., 2002. *Fundamentals of Heat and Mass Transfer*, fifth ed. John Wiley & Sons, Inc.

[20] Bove, R., Lunghi, P., and Sammes, N. M., 2005. "Sofc mathematic model for systems simulations - part 2: Definition of an analytical model". *International Journal of Hydrogen Energy*, **30**, pp. 189–200.

[21] Khalil, H. K., 2002. *Nonlinear Systems*, third ed. Prentice Hall.